

Turning high electrical conductive additive carbon black
to supercapacitor active materials: Effects of oxygen-
containing groups and electrolytes

Nutthaphon Phattharasupakun,^a Juthaporn Wutthiprom,^a Phansiri Suktha,^{a,b} Pawin

Iamprasertkun,^{a,b} Narong Chanlek,^c Celine.Shepherd,^d Emina.Hadzifejzovic,^d Mark G. Moloney,^d

John S. Foord,^d and Montree Sawangphruk^{a,}*

^aDepartment of Chemical and Biomolecular Engineering, School of Energy

Science and Engineering, Vidyasirimedhi Institute of Science and Technology,

Rayong 21210, Thailand

^bDepartment of Chemical Engineering, Centre for Advanced Studies in Nanotechnology and Its

Applications in Chemical Food and Agricultural Industries, and NANOTEC-KU-Centre of

Excellence on Nanoscale Materials Design for Green Nanotechnology, Kasetsart University,

Bangkok 10900, Thailand

^cSynchrotron Light Research Institute (Public Organization), 111 University Avenue, Muang

District, Nakhon Ratchasima 30000,

^dDepartment of Chemistry, Chemistry Research Laboratory, University of Oxford, Mansfield

Road, Oxford OX1 3TA, U.K.

KEYWORDS: Carbon black nanoparticles; Oxidized carbon nanosheets; Ionic liquid electrolyte,
Electrical double layer capacitors

ABSTRACT

Although carbon black nanoparticles (CBs) at ca. 10 wt.% are widely used as a conductive additives for energy storage electrodes for lithium ion batteries and supercapacitors, they are not extensively used as the active materials for such devices due to their poor ionic conductivity and wettability. In this work, CBs were oxidized by a process of refluxing with conc. HNO_3 for 6-72 h, providing oxidized CBs (OCBs) with different oxygen-containing groups (i.e., carboxyl, hydroxyl, and carbonyl) and contents. The OCBs refluxed for 12 h have ca. 2.0-fold higher accessible active surface area than that of the pristine CBs. The as-fabricated symmetric supercapacitor using OCBs refluxed for 12 h with a [BMP][DCA] ionic liquid electrolyte exhibits specific energy and maximum specific power of 88 Wh kg^{-1} and 8429 W kg^{-1} , respectively with the capacitance retention over 97% after 6000 cycles. A single coin-cell supercapacitor prototype fully charged can supply electrical power to a red LED over 24 min. This device may be practically used as a battery replacement in high power applications.

INTRODUCTION

Electrochemical capacitors or supercapacitors are of interest as promising energy storage devices and may find use in many applications such as uninterruptible power supply (UPS), security alarm systems, and hybrid electric vehicles (HEVs)^{1,2}. There are two major types of supercapacitors i.e., electrical double layer capacitors (EDLCs) and pseudocapacitors. EDLCs store charge electrostatically via the physical adsorption of solvated ions on the surface of the electrode leading to high charge/discharge rate, high specific power of 10 kW kg^{-1} and long cycle life ($>10^6$ cycles) when compared to batteries which have lower power density ($<1000 \text{ W kg}^{-1}$)^{1,3}. Typically, carbon materials e.g. activated carbons⁴, carbon nanotubes⁵, and graphene^{6,7} are used as the EDLC electrodes owing to their high surface area and high electrical conductivity. However, these carbon materials still suffer from high activation temperature ($\sim 600\text{-}1200^\circ\text{C}$), complex synthesis routes, and restacking^{6, 8,9}.

Carbon Black nanoparticles (CBs) are widely used at a loading content of ca. 10 wt.% as the conductive additive for fabricating the electrodes of supercapacitors, lithium ion batteries, and fuel cells¹⁰⁻¹⁴ because of their high electrical conductivity ($\sim 1\text{-}6 \text{ S cm}^{-1}$)¹⁵⁻¹⁶. However, CBs are not widely used as the active materials of energy storage devices due to their poor ionic conductivity, low surface area, and hydrophobic nature. As the result, they can only store little charge via electrochemical double-layered capacitance. Previously, the supercapacitor of highly graphitized CB (PureBlack 205) was studied in $1.5 \text{ M NEt}_4\text{BF}_4$ organic electrolyte exhibiting a specific capacitance (SC) of 2 F g^{-1} at 5 mA cm^{-2} ¹⁷. The supercapacitor of CBs (Cabot Corporation) exhibited a SC of 115 F g^{-1} at 20 mV s^{-1} in $1 \text{ M PC-Et}_4\text{NBF}_4$ organic electrolyte¹⁸. The supercapacitor of CBs (ENSACO 114 MM) showed a SC of 250 F g^{-1} at 34 mA cm^{-2} in 12 M

H₂SO₄¹⁹. As a result, CB-based supercapacitors cannot compete with the supercapacitors using other carbon-based materials e.g., graphene, carbon aerogel, activated carbon, and carbide-derived carbon²⁰⁻²³.

In this work, the CBs were oxidized by refluxing with conc. HNO₃ for 6-72 h. The oxidized CBs (OCBs) were then used as the active materials for supercapacitor electrodes. In order to achieve wide working potential (ca. 4 V) and high specific energy, 1-butyl-1-methylpyrrolidinium dicyanamide ([BMP][DCA]) ionic liquid was also used. To the best of our knowledge, ionic liquid-based supercapacitors of CBs and OCBs have not yet been reported. For comparison, other electrolytes including acidic, basic, and neutral electrolytes were also studied.

The as-fabricated coin-cell supercapacitors of OCBs exhibit the SC of 301 F g⁻¹ at an applied current of 1 mA per a cell (0.6 A g⁻¹), a specific energy of 88 Wh kg⁻¹, a maximum specific power of 8429 W kg⁻¹, and capacitance retention over 97% after 6000 charge/discharge cycling. This performance is much higher than that of other previous CB-based supercapacitors^{20, 24}. The supercapacitor prototype fully charged in this work can supply power to a red LED over 24 min, demonstrating that it may be practically used in many high energy applications.

EXPERIMENTAL SECTION

Chemicals and materials. Carbon black powder namely Super P (TIMCAL AMERICA INC.), sulphuric acid (H₂SO₄ 98%, QRec), nitric acid (HNO₃ 65%, QRec), 1-Methyl-2-Pyrrolidone (NMP 99.5%, QRec), 1-Butyl-1-methylpyrrolidinium dicyanamide ([BMP][DCA] 97%, Sigma-Aldrich),

and poly(vinylidene fluoride) (PVDF, Sigma-Aldrich, Mw~534,000) were of analytical reagent grade and used without further purification. Carbon fibre paper (CFP) was supplied from SGL Carbon SE (Germany) and used as the current collector. Hydrolysed PE film with a thickness of 25 mm was purchased from Gelon, Hong Kong. Deionized water (DI) with a resistance of 15 MΩ.cm through Millipore system (Milli-Q) was used in all experiments.

Oxidation of carbon black nanoparticles. The OCBs were synthesized by the process of refluxing with concentrated nitric acid. Briefly, 1-g CB was dispersed in 80 ml nitric acid and stirred for 1 h. The mixture suspension was transferred to a reflux condenser apparatus with a 250-ml round-bottom flask and then heated at 100 °C for 6 h. Note, the reaction time was varied from 6, 12, 24, 48, and 72 h for which the resulting products were denoted as OCB-6h, OCB-12h, OCB-24h, OCB-48h, and OCB-72h, respectively. For the purification, the suspension was washed with deionized water several times. The diluted suspension was centrifuged at 10000 rpm until neutral (pH 7) with deionized water and dried at 50 °C overnight.

Morphological and structural characterizations. The morphologies of CB and OCBs were characterized by transmission electron microscope (TEM, Hitachi, operated at 120 kV). The functional groups of OCBs were characterized by Fourier transform infrared spectrometer (FT-IR, PerkinElmer) and X-ray photoelectron spectroscopy (XPS, Axis Ultra DLD, Kratos Analytical Ltd., with Al-K alpha radiation ($h\nu = 14,866$ eV)). The structures of all OCBs were studied by

Raman spectroscopy (Senterra Dispersive Raman Microscope, Bruker) with an excitation wavelength of 532 nm and X-ray diffraction (XRD, Bruker, D8 Advance) using a Cu K α radiation (λ = 1.54056 Å). N₂ sorption/desorption isotherm was performed at 77 K (BELSORP-mini, MicrotracBEL Corp.) using Brunauer-Emmett-Teller (BET) method to determine the specific surface area of OCBs.

Methylene blue absorption. The as-prepared materials were dispersed in a standard aqueous solution of methylene blue (MB) in a ratio of 1 mg: 1 ml by ultrasonication for 2 h and stirred for 24 h to reach the absorption equilibrium. The supernatant suspensions were collected by a centrifugal and the MB concentration was measured by UV-vis-NIR spectrophotometer (PerkinElmer, Lambda 1050). The specific surface area (SSA) for MB liquid adsorption was calculated by the following equation (1)²⁵⁻²⁶;

$$SSA = \frac{N_A A_{MB}}{M_{MB}} \frac{(C_0 - C_e)V}{m_s} \quad (1)$$

where N_A is the Avogadro's number (6.02×10^{23} mol⁻¹), A_{MB} is the covered area per MB molecule (~ 1.35 nm²), M_{MB} is the molecular weight of MB (355.89 g mol⁻¹), C_0 and C_e are the initial and equilibrium concentrations of MB, respectively, V is the volume of MB, and m_s is the mass of the samples.

Fabrication of the supercapacitors and electrochemical evaluation. The electrodes were prepared by dispersing the active materials (i.e., OCBs), conductive carbon black, and PVDF

binder in a weight ratio of 8:1:1 in NMP and then sonicated for 1 h to form a slurry. The homogeneous slurry was sprayed on the CFP by an airbrush (Paasche Airbrush Company, USA) under a pressure of 30 psi and dried at 60 °C overnight. The symmetric supercapacitor cells were assembled in CR2016 coin cells via a hydraulic press at 800 psi for 5 s. The hydrolysed PE film with a thickness of 25 µm was used as the separator. The ionic liquid electrolyte is [BMP][DCA]. The amount of active material on each circle electrode with a diameter of 1.58 cm is about 1.0-1.5 mg.

Galvanostatic charge-discharge was tested using a NEWARE (Gelon) battery test system. Cyclic voltammetry (CV) was carried out using a Metrohm AUTOLAB potentiostat (PGSTAT 302N) at the scan rates of 10-100 mV s⁻¹. Electrochemical impedance spectra (EIS) was conducted with an applied amplitude of 0.01 V at the frequency range of 1 mHz - 100 kHz on a Metrohm AUTOLAB potentiostat (PGSTAT 302N).

RESULTS AND DISCUSSION

A TEM image in Figure 1a shows that the CBs have a spherical shape a particle size of ca. 50 nm, but are aggregated together forming a chain-like structure, and leading to high conductivity. TEM images of OCBs produced by refluxing for 6-72 h are shown in Figure 1b-f, respectively; in these cases, broken spheres of OCBs with a sheet-like structure are observed.

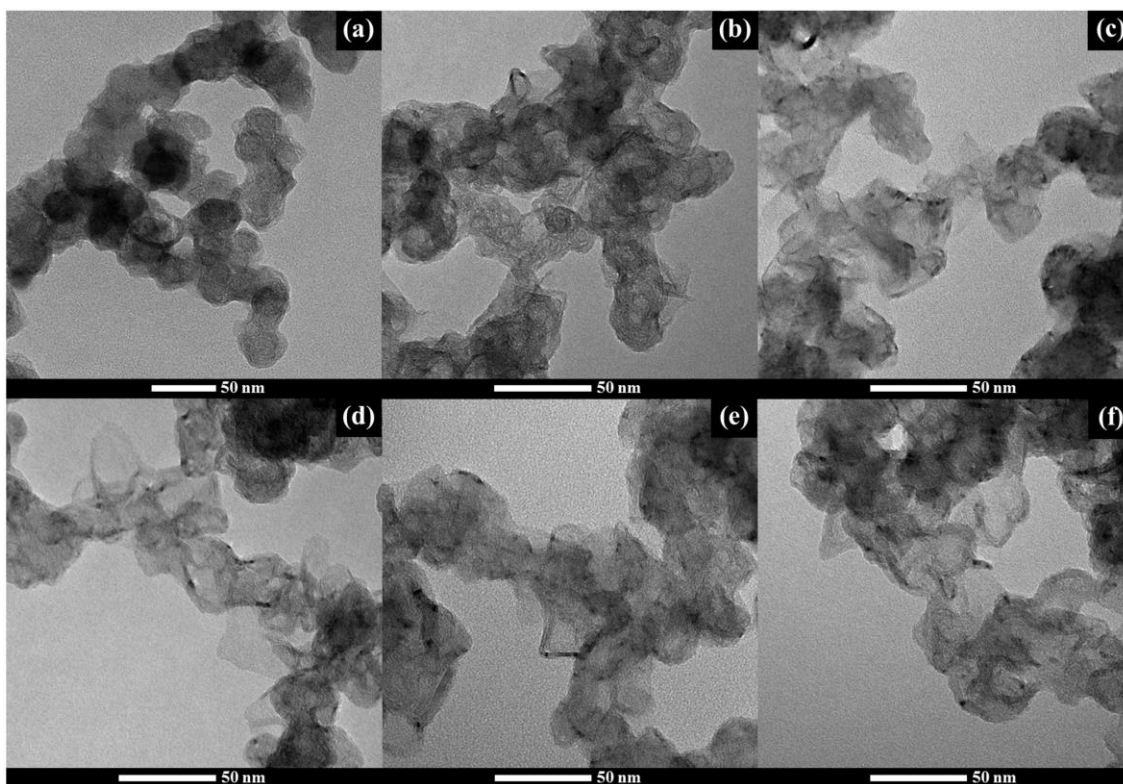
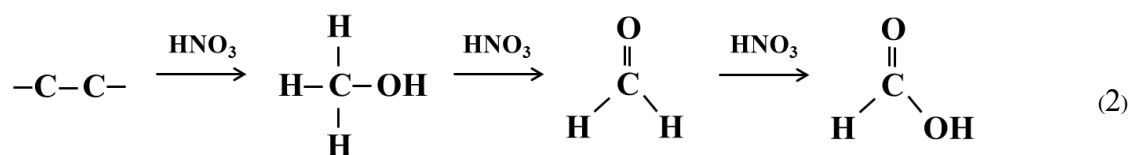


Figure 1. TEM images of (a) CB, (b) OCB-6h, (c) OCB-12h, (d) OCB-24h, (e) OCB-48h, and (f) OCB-72h.

The oxygen-containing functional groups on the surfaces of the OCBs were investigated by XPS is shown in Figure 2a. A wide-scan spectrum of pristine CB exhibited a carbon peak with a small content of oxygen. In contrast, the OCB-12h contained both carbon and oxygen owing to the oxygen functional groups on its surface. The C1s spectrum of CB (Figure 2b) can be divided into four peaks which are C-C, C-O, C-O-C with π - π^* signals located at 284.80, 285.53, 286.66, and 290.62 eV, respectively. It is well known that diluted volatile oxygen species can adsorb on the surface of the CBs. The C1s spectra of the OCB-12h in Figure 2c shows peaks at 284.79 eV, which belong to -C-C- and other peaks due to C-O (at 285.05 eV), C-O-C (at 286.26 eV), C=O (at

286.78 eV), and O-C=O (at 289.06 eV). The $\pi\text{-}\pi^*$ at 291.31 eV corresponds to π electrons delocalized in the benzene ring network in the structure of OCB. Figure 2d shows a narrow-scan O1s spectrum of OCB-12h, which was deconvoluted to three peaks of O=C-OH (at 531.14 eV), C=O (at 532.07 eV), and C-OH (at 533.55 eV). According to the XPS data, the O:C atomic ratios of CB, OCB-6h, OCB-12h, OCB-24h, OCB-48h, and OCB-72h are 0.0041, 0.0504, 0.0660, 0.1189, 0.1604, and 0.1905, respectively. The presence of the oxygen-containing functional groups can act as the electrochemically active sites, leading to faster charge mobility of ions into the material; this increases the ionic conductivity of the materials. Table 1 shows the surface composition of CB and OCBs determined by the XPS C1s spectra. The nitric acid oxidation starts from the decomposition of nitric acid into nitrogen oxide and nitrogen dioxide as well as oxygen. These compounds attack the aromatic rings in the structure of the CBs resulting in the oxidation of hydrocarbon into C-O (alcohol, phenol, and aliphatic ether) leading to the decrease in -C-C-/-C=C- bond content. Increasing the oxidation time can lead to high amount of oxygen-containing groups due to further oxidation into carbonyl and carboxyl groups, respectively. The $\pi\text{-}\pi^*$ bonds decrease as the oxidation process proceeds due to the substitution of oxygen functional groups into the benzene ring networks of carbon atoms. The oxidation in nitric acid pathways is shown in the following Eq. (2).



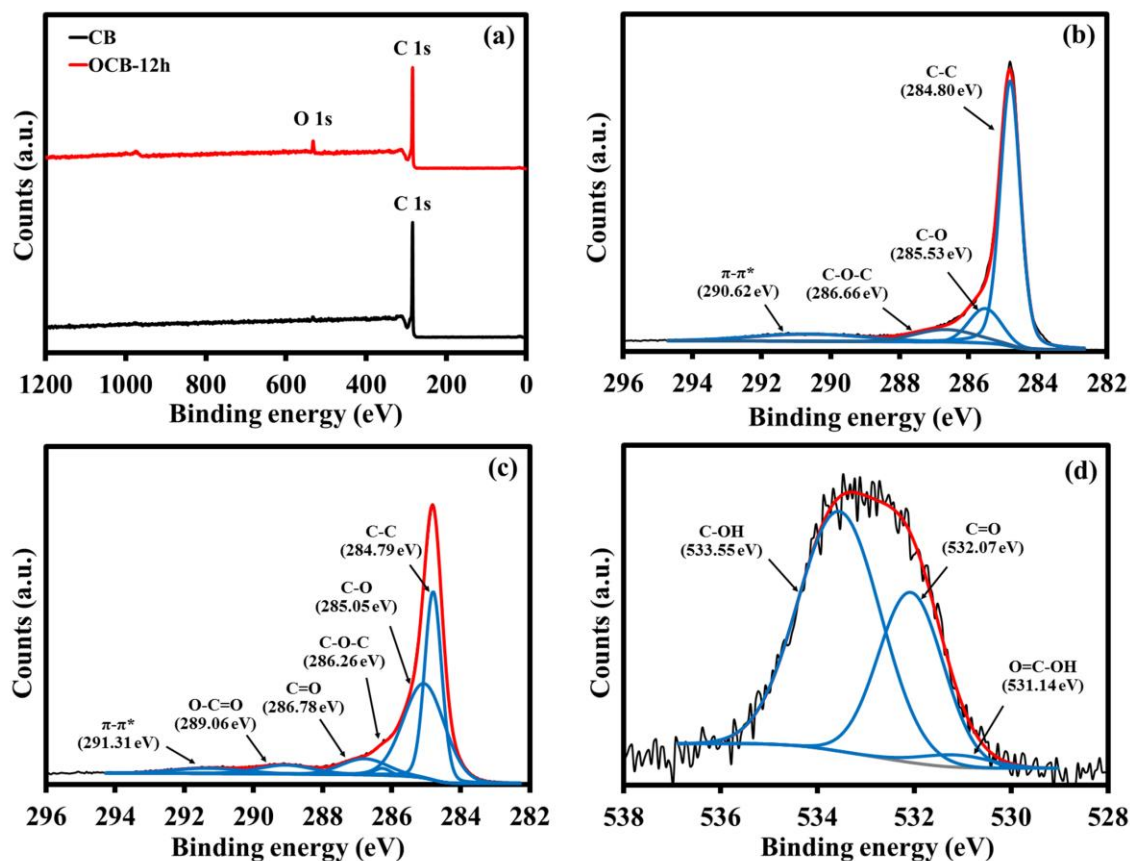


Figure 2. (a) Wide-scan XPS spectra of CB and OCB-12h, (b) narrow-scan C1s XPS spectrum of CB, (c) narrow-scan C1s XPS spectrum of OCB-12h, and (d) narrow-scan O1s XPS spectrum of OCB-12h.

Table 1. The surface composition of CB and OCBs determined by the XPS C1s spectra.

Samples	C-C (%)	C-O (%)	C-O-C (%)	C=O (%)	O-C=O (%)	π - π^* (%)
CB	68.66	12.93	9.16	0	0	9.23
OCB-6h	36.49	33.86	0.82	17.33	4.88	6.61

OCB-12h	36.94	43.87	1.17	8.16	5.52	4.34
OCB-24h	35.41	47.90	3.05	4.33	6.53	2.78
OCB-48h	36.92	44.37	2.25	4.92	8.27	3.26
OCB-72h	36.51	42.31	10.43	6.29	3.69	0.77

Raman spectra were carried out to study the characteristic and defect information of CB and OCBs. Both CB and OCBs display three obvious peaks, which are the typical feature of carbon-based materials. The D band around 1340 cm^{-1} is attributed to the structural disorder or defect in carbon atoms. The higher degree of oxidation, the more defect in the structure. The G band around 1570 cm^{-1} corresponds to the graphitic structure of carbon. The intensity ratios of D band to G band (I_D/I_G) of CB, OCB-6h, OCB-12h, OCB-24h, OCB-48h, and OCB-72h are 1.03, 1.08, 1.10, 1.14, 1.18, and 1.29, respectively. The 2D band, which describes the layer thickness of carbon materials, can be clearly seen around 2680 cm^{-1} for the OCB samples, indicating that the spherical structure of carbon black was disrupted, which is in good agreement with TEM^{27,28}. In addition, the FT-IR spectra were measured to confirm the functional groups on the OCB materials as shown in Figure 3b. The C-O ($\sim 1200\text{ cm}^{-1}$) and C=O ($\sim 1720\text{ cm}^{-1}$) stretching modes are clearly seen in OCBs samples, while the peaks of C=C ($\sim 1560\text{ cm}^{-1}$) and C-H ($\sim 2650\text{ cm}^{-1}$) stretching vibrations can be observed for both CB and OCBs samples. An XRD analysis was carried out to study the crystallographic structure of the materials. Both CB and OCBs show the diffraction

peaks at 2θ around 25° and 43° , which correspond to (002) and (100) crystallographic planes, respectively.

Figure 3d shows the UV-vis absorption spectra in standard methylene blue solution (100 ppm). The absorption intensities of OCBs at 665 nm are lower than the CB, indicating that the OCBs have more accessible surface area after the acid treatment. The calculated surface areas from MB absorption of CB, OCB-6h, OCB-12h, OCB-24h, OCB-48h, and OCB-72h are 86, 215, 183, 211, 216, and 217 $\text{m}^2 \text{g}^{-1}$, respectively. N_2 sorption isotherms and other properties of the as-prepared materials (i.e., BET, L_c , and d_{spacing}) are shown in Figure S1 and Table S1, respectively. Can you calculate the surface area from the BET data??

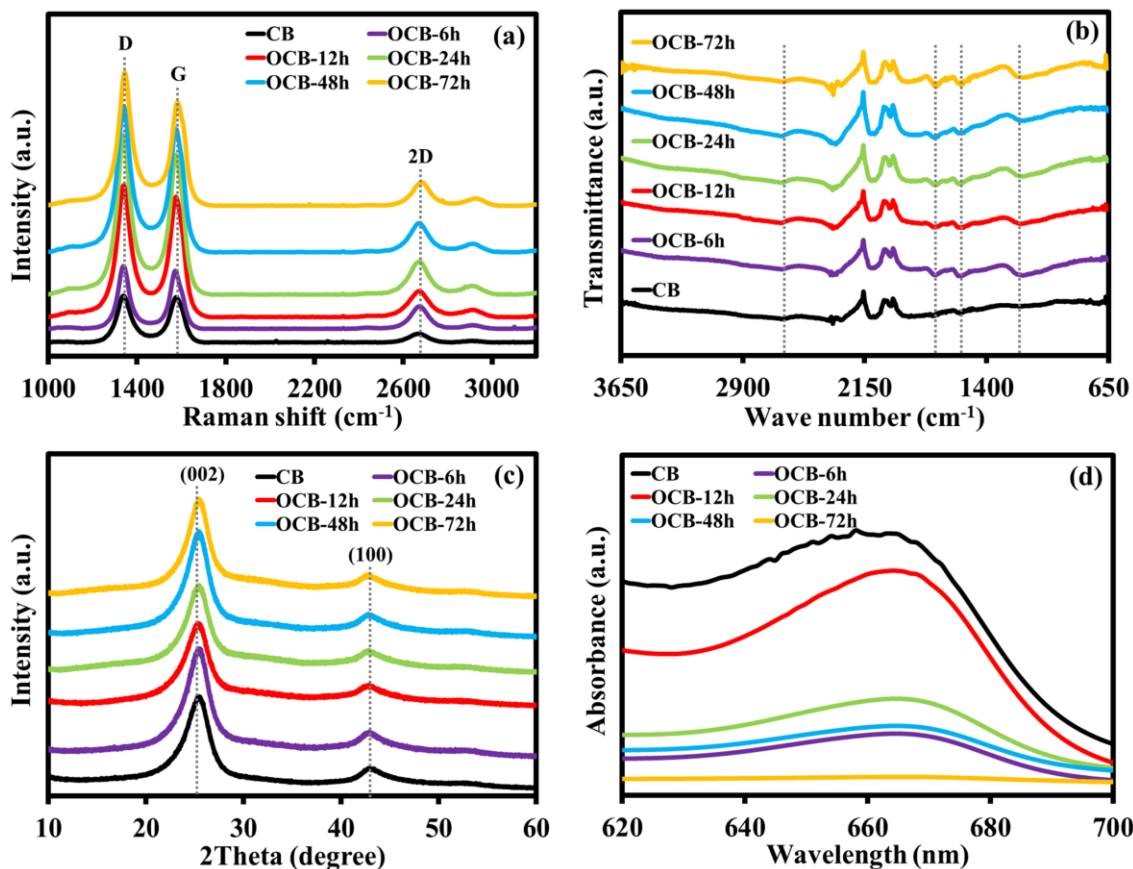


Figure 3. (a) Raman spectra, (b) FT-IR spectra, (c) XRD patterns, and (d) UV-vis absorption spectra in methylene blue solution of CB and OCBs, respectively.

Figure 4a shows the cyclic voltammetry (CV) of CB and OCB symmetric supercapacitors in the overall potential range of 4.0 V (from 0 to 4.0 V) in a [BMP][DCA] ionic liquid electrolyte at a scan rate of 100 mV s⁻¹. There are some broad redox peaks in the CV curves resulting from the oxygen-containing functional groups on the active materials (OCBs) that act as pseudo-capacitive materials. The CV curves of OCBs show higher current density and specific capacitance than the pristine CB at all scan rates, which are shown in Figure 4b. Moreover, the specific capacitance is almost the same when the scan rates increase, indicating an excellent capacitive behaviour, good stability and fast diffusion of ions in the electrolyte. The Galvanostatic charge-discharge (GCD) was also carried out to evaluate the performance of supercapacitors as shown in Figure 4c. At a cut-off potential of 3.0 V and an applied current of 1 mA, the OCB-12h exhibits the highest discharge time when compared to other materials. The small *iR* drop is observed for all curves, which is the characteristic of the ionic liquid-based electrolyte. The oxygen-containing functionalities on the surface of the OCBs cause the deviation in charge/discharge cycling due to the redox reaction. The specific capacitance vs. applied currents is shown in Figure 4d. The OCB-12h exhibits a capacitance of 301.5 F g⁻¹, which is 2.3-fold higher than that of the CB at an applied current of 1 mA (0.6 A g⁻¹). The specific capacitances of the OCB-6h, OCB-24h, OCB-48h, and OCB-72h are 194.0, 251.1, 233.6, and 186.9 F g⁻¹, respectively.

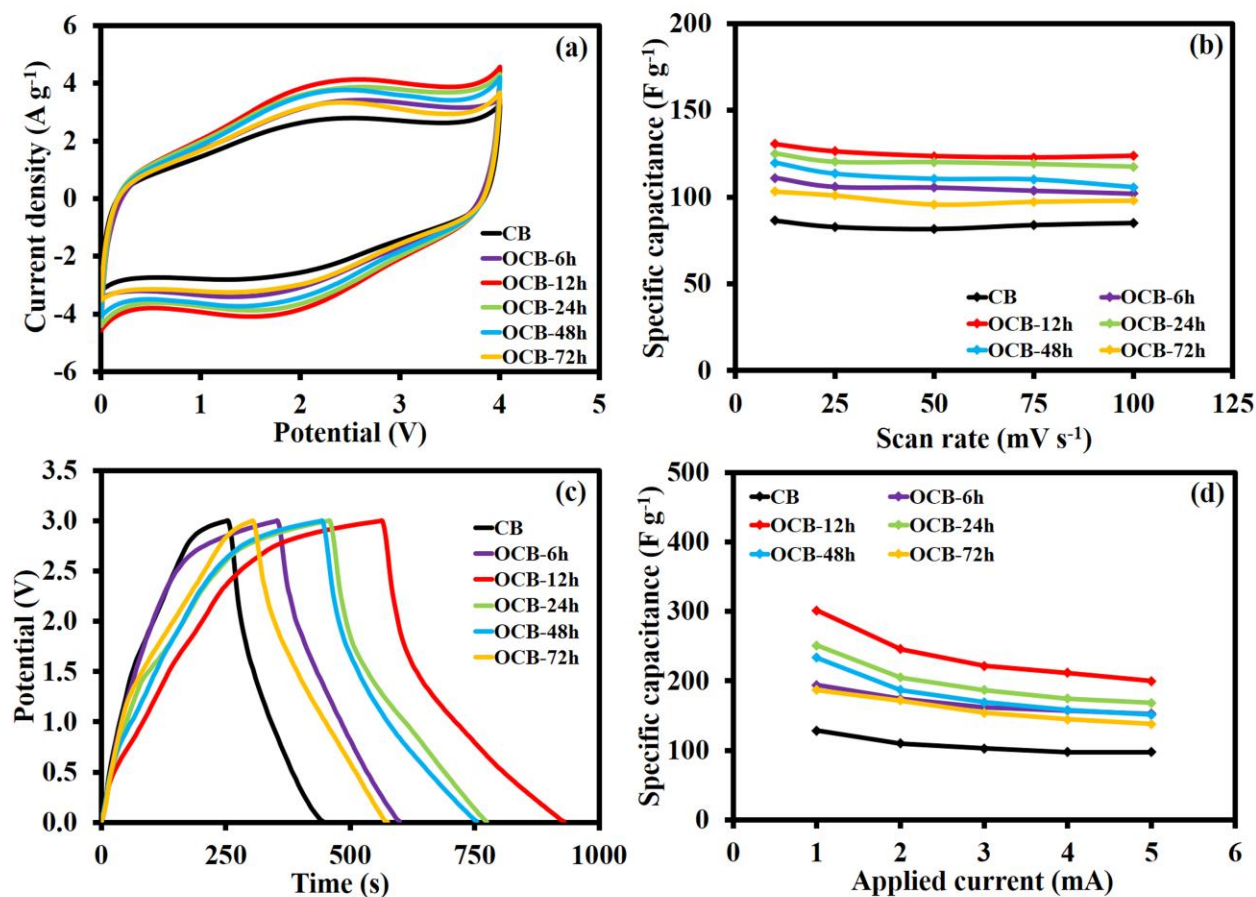


Figure 4. (a) CVs at a scan rate of 100 mV s⁻¹, (b) the specific capacitances as a function of the scan rates, (c) GCDs at an applied current of 1 mA a cell (0.6 A g⁻¹), and (d) the specific capacitances as a function of the applied currents of the CB and OCB supercapacitors.

The electrochemical impedance spectroscopy (EIS) of CB and OCB supercapacitors was also evaluated in a frequency range of 1 mHz – 100 kHz with an AC amplitude of 10 mV as shown in Figure 5a. All curves exhibit a 45° Warburg region in a medium-frequency region and also the nearly vertical line in a low-frequency region, indicating the low diffusion resistance of ions in the electrolyte and ideal capacitor behaviour. The inset image shows the high-frequency region of

the spectra. The interception in the X-axis represents the internal resistance (R_s) which is the resistance arising from the electrolyte, both in the electrode and separator, internal resistance of active materials, and the contact resistance in the system. The OCB-12h supercapacitor exhibits the lowest R_s (2.87 Ω), which is a typical value of the ionic liquid electrolyte, indicating that the oxygen functional groups can increase the wettability and ionic diffusivity in the electrode. The diameter of the semi-circle is a charge-transfer resistance (R_{ct}), which is attributed to the charge transfer between the interface of the electrode and electrolyte. The smaller semi-circle, is the higher mass transfer rate of ions into the materials. The OCB-12h supercapacitor exhibits the smallest R_{ct} (3.50 Ω) because of the oxygen functionalities on the surface that can help attract the ions in the electrolyte. The specific capacitance vs. the applied frequency is shown in Figure 5b. At the lowest frequency of 1 mHz, the OCB-12h supercapacitor exhibits a specific capacitance of 119.3 F g⁻¹, which is in good agreement with the CV and GCD results. The specific capacitances decrease as the applied frequency increases because at high frequency, since only some part of active materials is accessible. A Ragone chart of the CB and OCBs supercapacitors is shown in Figure 5c. The OCB-12h supercapacitor also delivers the maximum specific energy of 88 Wh kg⁻¹ and the maximum specific power of 8429 W kg⁻¹ when compared with other OCB supercapacitors. The capacitance retention of CB and OCB-12h supercapacitors in the ionic liquid electrolyte was evaluated by the GCD at an applied current of 5 mA a cell and shown in Figure 5d. After 6000 cycles, the capacitance retentions of CB and OCB-12h are over 80 and 97 %, respectively, indicating the excellent cycle stability of the supercapacitor devices. The

calculation details can be found in Eqs. S1-S6 in the Supporting Information. In addition, the effect of the electrolytes in the OCB-12h symmetric supercapacitors was also studied as shown in Figure S2 and S3. Among different types of electrolytes, the H_2SO_4 electrolyte exhibits the highest specific capacitance resulting from the faradaic redox reactions of surface oxygen functional groups as following Eqs. (3), (4), and (5)²⁹⁻³⁰ but the ionic liquid provides the widest working potential. Overall, the ionic liquid-based supercapacitor can provide the highest specific power and energy.

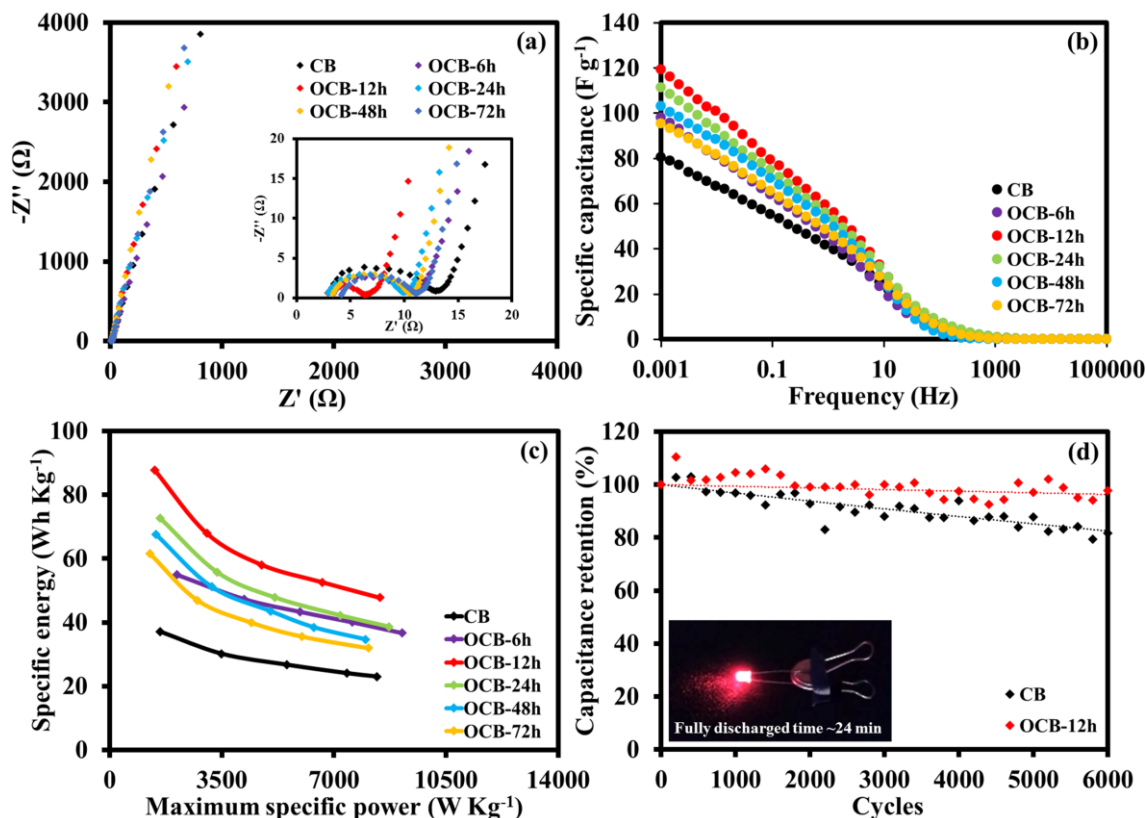
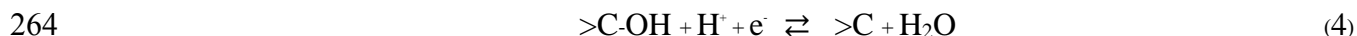
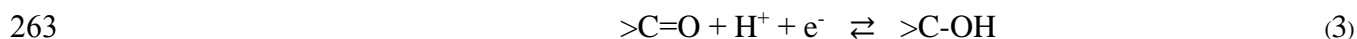


Figure 5. (a) Nyquist plots, (b) specific capacitances vs. applied frequency plots, (c) Ragone plots, and (d) the capacitance retention over 6000 cycles of CN, and OCBs, respectively.



266

267 CONCLUSIONS

268 As the CBs have rather low ionic conductivity and store little charges, they are typically used
 269 as the conductive additives for the battery and supercapacitor electrodes. In this work, the OCBs
 270 were successfully synthesized via the oxidation process by refluxing CBs with concentrated
 271 nitric acid for 12 h and used as the active electrode material of the supercapacitors. The
 272 increased active surface area and oxygen functional groups of OCBs can significantly improve
 273 the charge storage performance of the OCB supercapacitors. The as-fabricated supercapacitor of
 274 OCB-12h in the [BMP][DCA] ionic liquid electrolyte provides 2.4-fold higher specific energy than
 275 that of the CB supercapacitor. The supercapacitor of OCBs also shows an excellent capacitance
 276 retention over 97% over 6000 cycles. Interestingly, a single coin-cell supercapacitor of OCB-12h
 277 (CR2016) can supply electricity to a red LED over 24 min implying the practical use of this
 278 device.

279

280 ASSOCIATED CONTENT

281 **Supporting Information.** The calculation details of the supercapacitors performances, N₂
 282 sorption isotherms of the as-prepared materials, the properties of as-prepared materials, the

electrochemical performance of the OCB-12h in different electrolytes, and the charge storage performances of the reported CB-based supercapacitors. This material is available free of charge via the Internet at <http://pubs.acs.org>.

AUTHOR INFORMATION

Corresponding Author

* Corresponding author. Tel: 66(0)33-01-4251. Fax: 66(0)33-01-4445. E-mail address: montree.s@vistec.ac.th (M. Sawangphruk).

Author Contributions

M.S. conceived and designed this work and wrote the paper; N.P. carried out the experiments (synthesis, fabrication, Raman, FTIR, and electrochemical evaluation), and J.W., and P. S performed XPS, XRD, TEM, and N₂ sorption. All authors participated in the analysis and discussion of the results.

The authors declare no competing financial interest.

ACKNOWLEDGMENT

This work was financially supported by the Thailand Research Fund and Vidyasirimedhi Institute of Science and Technology (RSA5880043).

302 REFERENCES

- 303 1. Frackowiak, E.; Béguin, F., Carbon materials for the electrochemical storage of energy in
304 capacitors. *Carbon* **2001**, *39* (6), 937-950.
- 305 2. Simon, P.; Gogotsi, Y., Materials for electrochemical capacitors. *Nat Mater* **2008**, *7* (11),
306 845-854.
- 307 3. Pandolfo, A. G.; Hollenkamp, A. F., Carbon properties and their role in supercapacitors.
308 *Journal of Power Sources* **2006**, *157* (1), 11-27.
- 309 4. Gamby, J.; Taberna, P. L.; Simon, P.; Fauvarque, J. F.; Chesneau, M., Studies and
310 characterisations of various activated carbons used for carbon/carbon supercapacitors. *Journal of*
311 *Power Sources* **2001**, *101* (1), 109-116.
- 312 5. An, K. H.; Kim, W. S.; Park, Y. S.; Moon, J. M.; Bae, D. J.; Lim, S. C.; Lee, Y. S.; Lee, Y. H.,
313 Electrochemical Properties of High-Power Supercapacitors Using Single-Walled Carbon
314 Nanotube Electrodes. *Advanced Functional Materials* **2001**, *11* (5), 387-392.
- 315 6. Zhu, Y.; Murali, S.; Stoller, M. D.; Ganesh, K. J.; Cai, W.; Ferreira, P. J.; Pirkle, A.;
316 Wallace, R. M.; Cychosz, K. A.; Thommes, M.; Su, D.; Stach, E. A.; Ruoff, R. S., Carbon-Based
317 Supercapacitors Produced by Activation of Graphene. *Science* **2011**, *332* (6037), 1537-1541.
- 318 7. Zhang, L. L.; Zhou, R.; Zhao, X. S., Graphene-based materials as supercapacitor
319 electrodes. *Journal of Materials Chemistry* **2010**, *20* (29), 5983-5992.
- 320 8. Wang, J.; Kaskel, S., KOH activation of carbon-based materials for energy storage.
321 *Journal of Materials Chemistry* **2012**, *22* (45), 23710-23725.
- 322 9. Sun, Y.; Wu, Q.; Shi, G., Graphene based new energy materials. *Energy & Environmental*
323 *Science* **2011**, *4* (4), 1113-1132.
- 324 10. Dunn, B.; Kamath, H.; Tarascon, J.-M., Electrical Energy Storage for the Grid: A Battery
325 of Choices. *Science* **2011**, *334* (6058), 928-935.
- 326 11. Phattharasupakun, N.; Wutthiprom, J.; Chiochan, P.; Suktha, P.; Suksomboon, M.;
327 Kalasina, S.; Sawangphruk, M., Turning conductive carbon nanospheres into nanosheets for high-
328 performance supercapacitors of MnO₂ nanorods. *Chemical Communications* **2016**, *52* (12), 2585-
329 2588.
- 330 12. Winter, M.; Brodd, R. J., What Are Batteries, Fuel Cells, and Supercapacitors? *Chemical*
331 *Reviews* **2004**, *104* (10), 4245-4270.
- 332 13. Pandolfo, A. G.; Wilson, G. J.; Huynh, T. D.; Hollenkamp, A. F., The Influence of
333 Conductive Additives and Inter-Particle Voids in Carbon EDLC Electrodes. *Fuel Cells* **2010**, *10*
334 (5), 856-864.
- 335 14. Spahr, M. E.; Goers, D.; Leone, A.; Stallone, S.; Grivei, E., Development of carbon
336 conductive additives for advanced lithium ion batteries. *Journal of Power Sources* **2011**, *196* (7),
337 3404-3413.
- 338 15. Marinho, B.; Ghislandi, M.; Tkalya, E.; Koning, C. E.; de With, G., Electrical conductivity
339 of compacts of graphene, multi-wall carbon nanotubes, carbon black, and graphite powder.
340 *Powder Technology* **2012**, *221*, 351-358.

16. Pantea, D.; Darmstadt, H.; Kaliaguine, S.; Roy, C., Electrical conductivity of conductive carbon blacks: influence of surface chemistry and topology. *Applied Surface Science* **2003**, *217* (1-4), 181-193.
17. Portet, C.; Yushin, G.; Gogotsi, Y., Electrochemical performance of carbon onions, nanodiamonds, carbon black and multiwalled nanotubes in electrical double layer capacitors. *Carbon* **2007**, *45* (13), 2511-2518.
18. Krause, A.; Kossyrev, P.; Oljaca, M.; Passerini, S.; Winter, M.; Balducci, A., Electrochemical double layer capacitor and lithium-ion capacitor based on carbon black. *Journal of Power Sources* **2011**, *196* (20), 8836-8842.
19. Beck, F.; Dolata, M.; Grivei, E.; Probst, N., Electrochemical supercapacitors based on industrial carbon blacks in aqueous H₂SO₄. *Journal of Applied Electrochemistry* **2001**, *31* (8), 845-853.
20. Iamprasertkun, P.; Krittayavathananon, A.; Sawangphruk, M., N-doped reduced graphene oxide aerogel coated on carboxyl-modified carbon fiber paper for high-performance ionic-liquid supercapacitors. *Carbon* **2016**, *102*, 455-461.
21. Huang, P.; Lethien, C.; Pinaud, S.; Brousse, K.; Laloo, R.; Turq, V.; Respaud, M.; Demortière, A.; Daffos, B.; Taberna, P. L.; Chaudret, B.; Gogotsi, Y.; Simon, P., On-chip and freestanding elastic carbon films for micro-supercapacitors. *Science* **2016**, *351* (6274), 691-695.
22. Dyatkin, B.; Gogotsi, O.; Malinovskiy, B.; Zozulya, Y.; Simon, P.; Gogotsi, Y., High capacitance of coarse-grained carbide derived carbon electrodes. *Journal of Power Sources* **2016**, *306*, 32-41.
23. Chmiola, J.; Yushin, G.; Gogotsi, Y.; Portet, C.; Simon, P.; Taberna, P. L., Anomalous Increase in Carbon Capacitance at Pore Sizes Less Than 1 Nanometer. *Science* **2006**, *313* (5794), 1760-1763.
24. Béguin, F.; Presser, V.; Balducci, A.; Frackowiak, E., Carbons and Electrolytes for Advanced Supercapacitors. *Advanced Materials* **2014**, *26* (14), 2219-2251.
25. Wang, Z.; Han, Y.; Zeng, Y.; Qie, Y.; Wang, Y.; Zheng, D.; Lu, X.; Tong, Y., Activated carbon fiber paper with exceptional capacitive performance as a robust electrode for supercapacitors. *Journal of Materials Chemistry A* **2016**, *4* (16), 5828-5833.
26. Yang, C.; Shen, J.; Wang, C.; Fei, H.; Bao, H.; Wang, G., All-solid-state asymmetric supercapacitor based on reduced graphene oxide/carbon nanotube and carbon fiber paper/polypyrrole electrodes. *Journal of Materials Chemistry A* **2014**, *2* (5), 1458-1464.
27. Ferrari, A. C.; Meyer, J. C.; Scardaci, V.; Casiraghi, C.; Lazzeri, M.; Mauri, F.; Piscanec, S.; Jiang, D.; Novoselov, K. S.; Roth, S.; Geim, A. K., Raman Spectrum of Graphene and Graphene Layers. *Physical Review Letters* **2006**, *97* (18), 187401.
28. Bokobza, L.; Bruneel, J.-L.; Couzi, M., Raman Spectra of Carbon-Based Materials (from Graphite to Carbon Black) and of Some Silicone Composites. *C* **2015**, *1* (1), 77.
29. Fan, L.-Z.; Qiao, S.; Song, W.; Wu, M.; He, X.; Qu, X., Effects of the functional groups on the electrochemical properties of ordered porous carbon for supercapacitors. *Electrochimica Acta* **2013**, *105*, 299-304.

30. Fan, X.; Lu, Y.; Xu, H.; Kong, X.; Wang, J., Reversible redox reaction on the oxygen-containing functional groups of an electrochemically modified graphite electrode for the pseudo-capacitance. *Journal of Materials Chemistry* **2011**, *21* (46), 18753-18760.

Graphical abstract

